

Research Article

Open Access



# A template-stripped carbon nanofiber/poly(styrene-butadiene-styrene) compound for high-sensitivity pressure and strain sensing

Yaoxu Xiong<sup>#</sup>, Zhiqiang Lin<sup>#</sup>, Zeyu Zhao, Yadong Xu, Yanjun Wan, Pengli Zhu, Yougen Hu<sup>\*</sup>, Rong Sun

Shenzhen Institute of Advanced Electronic Materials, Shenzhen Institute of Advanced Technology, Chinese Academy of Sciences, Shenzhen 518055, Guangdong, China.

<sup>#</sup>Authors contributed equally.

<sup>\*</sup>**Correspondence to:** Dr. Yougen Hu, Shenzhen Institute of Advanced Electronic Materials, Shenzhen Institute of Advanced Technology, Chinese Academy of Sciences, 1068 Xueyuan Avenue, Nanshan District, Shenzhen 518055, Guangdong, China. E-mail: yg.hu@siat.ac.cn

**How to cite this article:** Xiong Y, Lin Z, Zhao Z, Xu Y, Wan Y, Zhu P, Hu Y, Sun R. A template-stripped carbon nanofiber/poly(styrene-butadiene-styrene) compound for high-sensitivity pressure and strain sensing. *Soft Sci* 2022;2:14. <https://dx.doi.org/10.20517/ss.2022.12>

**Received:** 7 Jun 2022 **First Decision:** 11 Jul 2022 **Revised:** 4 Aug 2022 **Accepted:** 15 Aug 2022 **Published:** 1 Sep 2022

**Academic Editor:** Zhifeng Ren **Copy Editor:** Fangling Lan **Production Editor:** Fangling Lan

## Abstract

Materials selection and microstructural design of the sensing part of flexible pressure sensors are of great significance in improving their performance. However, achieving synergy between the sensing material and the microstructure of the flexible sensors remains a challenge. Herein, compressible and stretchable sensors based on a carbon nanofiber/poly(styrene-butadiene-styrene) (CNF/SBS) compound are demonstrated with a template-stripped method for detecting various human motions, including pulses, finger bending and pressure distributions. Benefiting from the adjustable fingerprint microstructure and mass fraction of CNFs, the as-designed flexible pressure sensor dramatically achieves a high sensitivity of 769.2 kPa<sup>-1</sup>, a low detection limit of 5 Pa and high reliability of over 1000 cycles. Moreover, the flexible sensor based on CNF/SBS can be stretched due to the outstanding tensile properties of SBS. The enhanced stretchable sensor remarkably possesses a high gauge factor of 105.6 with a stretch range of 0%-300% and up to 600% elongation. Importantly, the proposed pressure and tension strain sensors are investigated to monitor vigorous human motion, revealing their tremendous potential for applications in flexible compressible and stretchable wearable electronics.

**Keywords:** Pressure sensors, stretchable sensors, high sensitivity, tactile application



© The Author(s) 2022. **Open Access** This article is licensed under a Creative Commons Attribution 4.0 International License (<https://creativecommons.org/licenses/by/4.0/>), which permits unrestricted use, sharing, adaptation, distribution and reproduction in any medium or format, for any purpose, even commercially, as long as you give appropriate credit to the original author(s) and the source, provide a link to the Creative Commons license, and indicate if changes were made.



## INTRODUCTION

Flexible electronics, which imitate the sensing function of human skin, have been attracting intensive interest as fundamental components of flexible displays, prostheses and wearable medical devices<sup>[1-7]</sup>. As wearable electric devices, flexible sensors should possess a low modulus and wide working range from subtle vibrations (e.g., pulses, < 1%) to large strains (e.g., joint movements, > 55%), similar to human skin. One of the major requirements is the ability to simultaneously receive and differentiate multiple pressure stimuli for skin-like flexible sensors. To accurately mimic sensing functions, four types of flexible sensors based on different signal transduction modes have been explored and applied, namely, piezoresistive, capacitive, piezoelectric and triboelectric sensors<sup>[1,4-6,8-15]</sup>. Due to their simple device structure and high stability, piezoresistive sensors, which convert mechanical deformation into electrical resistance or current change, are commonly applied as sensing components<sup>[16-21]</sup>.

The sensing performance is closely associated with the microstructural (e.g., shape, size and distribution) and material properties (e.g., thickness, Young's modulus and Poisson's ratio). Recently, significant efforts have been devoted to enhancing the sensitivity, linear detection range, *etc.*, through materials optimization and structural design. Notably, it has been illustrated that various microstructural designs, including pillar<sup>[22-24]</sup>, convex<sup>[7,25-27]</sup>, pyramid<sup>[28-30]</sup>, wave<sup>[31,32]</sup> and three-dimensional network structures<sup>[33-35]</sup>, are effective strategies to acquire highly sensitive flexible piezoresistive sensors. For example, Cao *et al.* reported a flexible tactile sensor based on single-walled carbon nanotubes/Polydimethylsiloxane (CNTs/PDMS) with micropyramid arrays by templating from a Si mold<sup>[28]</sup>. The sensor showed a high-pressure sensitivity of 3.26 kPa<sup>-1</sup> at 300 Pa and could detect the shear force changes induced by the dynamic interaction between the sensor and the tested material surface. Pang *et al.* prepared a pressure sensor based on rGO/PMDS with the use of sandpaper as a template and a thermal reduction method<sup>[36]</sup>. The randomly distributed bulge enabled the sensitivity of the pressure sensor to reach 25.1 kPa<sup>-1</sup> with a linearity range of up to 2.6 kPa. Wang *et al.* fabricated a pressure sensor based on a hemisphere array via an inversely templating concave structure derived from the breath figure method<sup>[26]</sup>. The interlocked subtle microstructure endowed a sensitivity as high as 196 kPa<sup>-1</sup> with a linearity range up to 10 kPa.

However, the flexible substrates of most pressure sensors are made of microstructured PDMS, and flexible electrodes are constructed by adsorbing the conductive layer on the surface of the PMDS. These pressure sensors exhibit narrow strain properties. Moreover, conductive polymer composites combining the electrical conductivity of fillers and flexible polymers are widely used to fabricate flexible stretch sensors. Typically, the conductivity of elastomeric composites is significantly enhanced by the mass fraction of conductive fillers, such as carbon nanotubes, carbon nanofibers (CNFs) and silver nanowires. For example, Hu *et al.* fabricated a conductive elastic composite of PS@Ag/PDMS, which exhibited a large workable strain range (> 80%) and high sensitivity gauge factors (GFs) of 17.5 at a strain of 10%, 6 at a strain of 10%-60% and 78.6 at a strain of 60%-80%<sup>[37]</sup>. Lai *et al.* fabricated ion gels consisting of a poly(acrylic acid) network and 1-ethyl-3-methylimidazolium dicyanamide<sup>[38]</sup>. The ion gel-based strain sensors exhibited high sensitivity (GF = 0.73) with a wide strain-sensing range (0%-750%) and excellent durability (1400 cycles). Therefore, conductive polymers provide a design for making flexible sensors that are both compressible and stretchable.

As one of the most important factors in protecting the body and perceiving external environments, especially the perception of pressure and temperature, the epidermis provides a bionic structural strategy

with its unique surface structure. Herein, a simple strategy to fabricate both compressible and stretchable sensing layers based on CNFs mixed with flexible styrene-block-butadiene-block-styrene (SBS) is presented. Inspired by the epidermis structure of human skin, a film based on CNF/SBS with randomly distributed ravine surfaces is fabricated by employing sandpaper as a template. Two layers of microstructured film are stacked face-to-face to design a flexible pressure sensor. Due to the efficient transition from the weak conductive to the conductive state via intersecting the CNF network of the electrical microstructured surface, the optimized pressure sensor exhibits ultrahigh sensitivity ( $769 \text{ kPa}^{-1}$  at 0-2 kPa), a fast response time (0.1 s) and good stability (1000 compressive cycles). Such a highly sensitive pressure sensor can detect subtle physiological real-time pulses and pressure distributions. Moreover, due to the outstanding tensile properties of SBS, the sensing layer based on CNF/SBS can also be used as a tensile sensor. Inspired by the “crack” structure of spider joints, Ag NPs are reduced *in situ* to form a similar “crack” structure on the CNF/SBS surface. The composite of Ag/CNF/SBS simultaneously exhibits a large strain range (600%), high sensitivity ( $GF = 105$  at 0%-250% and 4646 at 500%-600%) and high stability (1000 cycles). The sensitivity and stretchability can be tuned by tailoring the mass fraction of CNFs and Ag. Based on this outstanding performance, the potential applications of the sensors in monitoring human movements and pressure distributions are further demonstrated.

## EXPERIMENTAL

### Materials

CNFs were purchased from Sigma (719781), SBS (CB20C) was obtained from Shenzhen Plastic Source Industrial Co., Ltd. and silver trifluoroacetate was purchased from Aladdin (S109509). The sandpaper and Ag wires were commercially available, and ethyl acetate ( $\text{CH}_3\text{COOC}_2\text{H}_5$ , > 99%) and ethanol ( $\text{C}_2\text{H}_5\text{OH}$ , > 70%) were supplied by Sinopharm Chemical Reagent Co., Ltd. (Shanghai, China) and used as soon as received. Ultrapure water ( $>18 \text{ M}\Omega \text{ cm}^{-1}$ ) was used for all experiments.

### Preparation of microstructured CNF/SBS films

Different commercial sandpapers (#400, #600, #1000 and #2000) were cleaned with ethanol and then dried for later use. The SBS particulates were completely dissolved into an ethyl acetate solution under magnetic stirring at 500 r/min. The CNFs were dispersed in another ethyl acetate solution by sonication for 30 min, and then the SBS solution (20 wt.%) was mixed with the CNF dispersed solution (5 wt.%) in different ratios to prepare CNF/SBS solutions with mass fractions of 2%, 3%, 4%, 5%, 7%, 10%, 15% and 20%, respectively. Finally, the prepared CNF/SBS solution was poured on the precleaned sandpaper and put into a vacuum desiccator to remove bubbles at room temperature. After complete evaporation of the ethyl acetate, the CNF/SBS film with microstructures was carefully peeled off from sandpaper and cut into dimensions of  $1.5 \text{ cm} \times 1 \text{ cm}$  for making pressure sensors.

### Preparation of flat CNF/SBS and Ag/CNF/SBS films

The as-prepared CNF/SBS solution (5 mL) was poured onto a smooth glass dish ( $5 \text{ cm} \times 5 \text{ cm}$ ) and then put into a vacuum desiccator to remove the bubbles at room temperature. After the ethyl acetate was completely evaporated, the CNF/SBS film was carefully peeled off from a smooth glass dish and cut into dimensions of  $1.5 \text{ cm} \times 1 \text{ cm}$  for stretch sensor use. The Ag/CNF/SBS film was fabricated by the *in situ* reduction of silver particles on the surface of the CNF/SBS film. The as-prepared CNF/SBS film was immersed into a silver trifluoroacetate/ethanol solution (15 wt.%) for 30 min and air dried for 3 h. It was then immersed into a hydrazine hydrate solution (50 wt.%) for 30 min. After being cleaned with deionized water and dried at  $50 \text{ }^\circ\text{C}$ , the prepared Ag/CNF/SBS film was cut into dimensions of  $1.5 \text{ cm} \times 1 \text{ cm}$  for stretch sensor use.

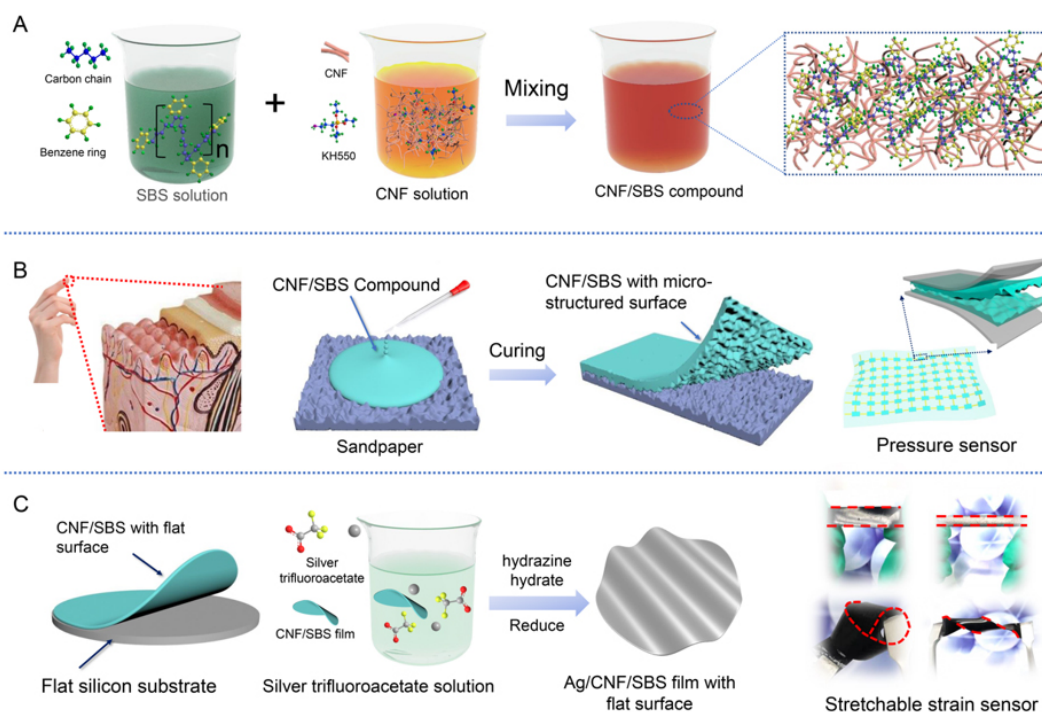


**Figure 1.** Fabrication of pressure and strain sensors. (A) Preparation of CNF/SBS dispersion solution; (B) structure of human skin and schematics for the preparation of pressure sensor composited with surface microstructured CNF/SBS; (C) preparation of high stretchable strain sensor with Ag/CNF/SBS composites.

### Fabrication of pressure and stretch sensors

The pressure sensors consisting of two microstructured CNF/SBS films (1 cm × 1 cm) were assembled with commercial flexible Ag wire electrodes, followed by sealing with scotch tape. The stretch sensors consisted of a single flat CNF/SBS film (1 cm × 1 cm) or flat Ag/CNF/SBS film (1 cm × 1 cm) with commercial flexible Ag wire electrodes.

### Characterization

The morphologies were characterized by field-emission scanning electron microscopy (FE-SEM, FEI Nano SEM 450). The resistance was measured by an Agilent 34401A multimeter. The applied pressure was determined using an electronic universal testing machine (Shimadzu AG-X Plus, 100 N). The current was measured by an electrochemical workstation (CHI 760e). The current-voltage characteristics of the sensors were detected by a semiconductor analyzer (Keithley, 4200-SCS).

## RESULTS AND DISCUSSION

Both the microstructured and flat CNF/SBS films were prepared using a template-stripped method with SBS/CNF solutions. A schematic for the fabrication of the SBS/CNF solutions is illustrated in Figure 1A. In order to acquire a uniform CNF/SBS dispersion, the CNF/ethyl acetate solution and silane stabilizer (KH550) were blended under ultrasonic conditions for 30 min. The SBS/ethyl acetate solution was then added and the blended solution was magnetically stirred for 1 h (the beaker should be sealed when stirring due to the volatilization of ethyl acetate). Inspired by the structure of human epidermis tissue [Figure 1B], microstructures were introduced to the surface of the CNF/SBS film with sandpaper as a template. The as-prepared CNF/SBS mixture solution was dipped on the sandpaper and heated at 60 °C for 1 h. After the ethyl acetate was volatilized completely, we could obtain the microstructured CNF/SBS film when it was

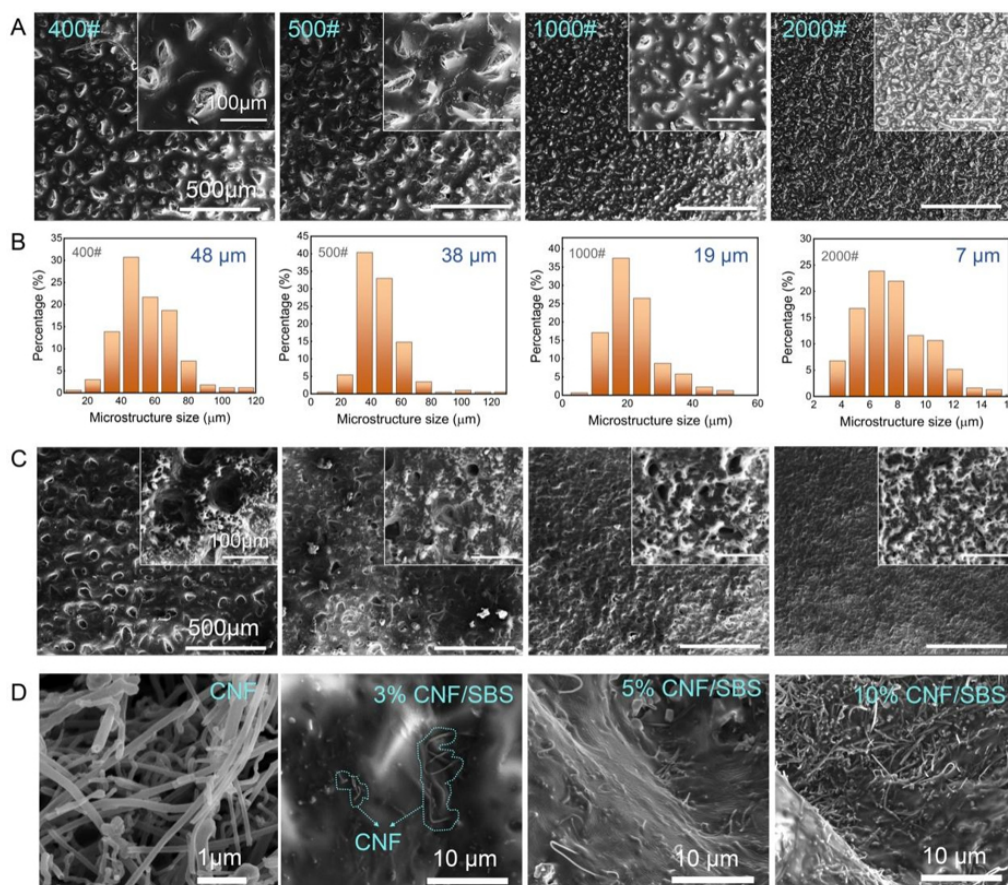


**Figure 2.** (A) SEM images of different size sandpapers, including 400#, 500#, 1000# and 2000#; (B) corresponding size of microstructural distribution of different sandpapers; (C) sample of CNF/SBS films fabricated with 400#, 500#, 1000# and 2000# sandpapers as templates; (D) SEM images of CNFs and CNF/SBS with mass fractions of 3%, 5% and 10%, respectively.

carefully peeled off from the sandpaper. The morphology of the microstructure can be tuned by applying sandpaper with different roughnesses (2000#, 1000#, 500# and 400#) as templates. Based on the CNF/SBS solutions, the Ag/CNF/SBS-based tension sensor can also be fabricated with a flat silicon wafer as a template. As shown in Figure 1C, similar to the fabrication process of microstructured CNF/SBS films, the flat CNF/SBS film can be obtained by using a flat silicon wafer instead of sandpaper as a template. The resulting Ag/CNF/SBS film can be easily bent and twisted, which demonstrates its excellent flexibility and stretchability.

To further investigate the relationship between the morphology and sensor performance, the surface roughness of the microstructured CNF/SBS film was controlled by using sandpaper with different grit numbers (400#, 500#, 1000# and 2000#, respectively). For the template-stripped method, the surface roughness of the template is closely related to the surface morphology of the as-prepared microstructured CNF/SBS film. As shown in Figure 2A, the surface morphology of the sandpaper with different grit numbers was characterized by SEM. Moreover, the particle sizes of the microstructures were counted and analyzed [Figure 2B]. As the grit numbers of sandpaper increased from 400# to 2000#, the average size of the microstructure gradually decreased from  $\sim 50$  to  $\sim 8$   $\mu\text{m}$ . The CNF/SBS film samples with microstructures fabricated by different sandpapers are shown in Figure 2C. Correspondingly, the average size of the microstructure of the CNF/SBS film decreases gradually as the average size of the microstructure

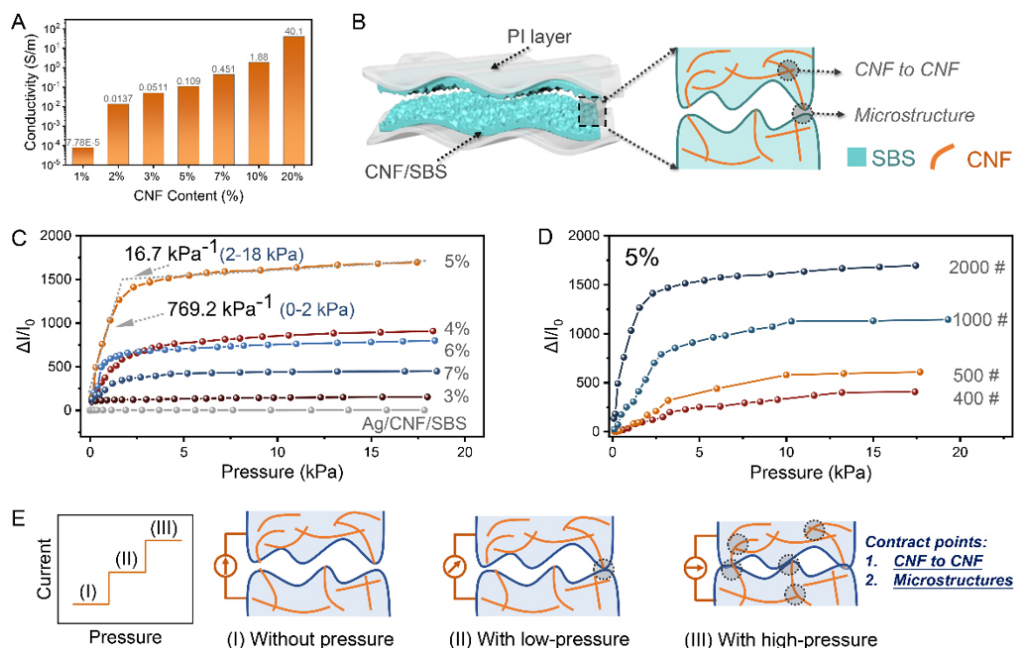


**Figure 3.** (A) Relational graph of volumetric conductivity and CNF mass fraction; (B) schematic of structure of microstructured CNF/SBS-based pressure sensor; (C) resistance variation of microstructured CNF/SBS-based pressure sensor with different CNF contents; (D) resistance variation of microstructured CNF/SBS-based pressure sensor with different microstructures; (E) working principle of microstructured CNF/SBS-based pressure sensor.

of the template used decreases. In addition, the average heights of the microstructure of the CNF/SBS films were 10, 25, 40 and 55  $\mu\text{m}$  when 2000#, 1000#, 500# and 400# sandpapers were used as templates, respectively [Supplementary Figure 1]. These results reveal that the microstructures of the CNF/SBS films can be easily controlled with templates with different grit numbers. This is, therefore, a facile, highly efficient and low-cost approach for constructing the microstructures of sensors.

Microstructural construction and materials selection are commonly applied to enhance the sensing performance of sensors. In addition to constructing microstructures using a template-stripped method, we further modified the electrical properties of the elastic SBS polymer matrix with conductive CNFs. Due to their high aspect ratio and conductivity [left of Figure 2D], CNFs are some of the most frequently used conductive fillers for piezoresistive-sensing materials. During deformation, CNFs with high aspect ratios can be interconnected with each other more easily, and therefore CNF-based polymers have greater variation in resistance. As the CNF content increases [right of Figure 2D], their distribution density in the SBS matrix increases significantly, which also improves the electrical interconnection between them.

To investigate the influence of CNF/SBS conductivity on pressure sensors, different resistances of CNF/SBS layers were fabricated by regulating the mass fraction of CNFs for comparison. Consequently, the conductivity of the CNF/SBS film demonstrated a positive relationship between the mass loading of CNFs with their conductivity. Typically, the conductivity of the CNF/SBS film increased with increasing CNF mass fraction due to the more interlaced conductive network formed. In particular, the conductivity of CNF/SBS changed significantly with a 3%-7% mass fraction of CNFs. As shown in Figure 3A, the conductivity of CNF/SBS was less than 0.0008 S/m when the CNF content was 1% and increased by more than 10,000 times to  $\sim 40$  S/m when the CNF content was raised to 20%. In conclusion, the piezoresistive properties of CNF/SBS can be controllably modulated by changing the CNF content. Figure 3B shows the

microstructured CNF/SBS-based pressure sensor assembled with two microstructured CNF/SBS films. It is noteworthy that the surfaces with microstructures were laminated to each other during the assembly process.

The CNF content significantly affected the resistance variation properties during deformation. [Figure 3C](#) shows the effect of different CNF mass fractions on the curve of current change rate-pressure. Interestingly, it demonstrates that the sensitivity of the sensor increases successively when the mass fractions of CNFs increase from 3% to 5%. However, when the mass fraction of CNFs continues to increase to 7%, the sensitivity of the sensor gradually decreases. This is because the CNF/SBS exhibited an obvious percolation threshold effect when the CNF content was higher than 5%. The sensitivity, which can be expressed as  $(I-I_0)/(I_0P)$ , is used to access the performance of a flexible sensor, where  $I$  and  $I_0$  are the current and initial current, respectively, and  $P$  is the applied pressure. Therefore, the sensor has a very high sensitivity when the mass fraction of CNFs is 5%, which is mainly because the conductivity has a significant impact on the sensitivity of the sensor. When the mass fraction of CNFs is less than 5%, the conductive network of the CNF/SBS sensor layer has many defects, which reduce the relationship between the conductivity and the change of contact area of the microstructure. Therefore, the sensitivity of the sensor increases with the improvement of the conductivity. When the mass fraction of CNFs exceeds 5%, due to the good conductive network of the sensor, the sensitivity is mainly controlled by the change of the contact area of the microstructure and conductivity contribute less to the sensitivity of the sensor. The increased conductivity of the sensing layer increases the initial current, which leads to the decrease of the sensitivity as the mass fraction of CNFs increases.

In addition, to investigate the significant influence of conductivity on sensitivity, a layer of highly conductive silver nanoparticles was reduced on the surface of the microstructured CNF/SBS film (with a CNF content of 5%) to obtain Ag/CNF/SBS comparison samples with high conductivity. Although the conductivity could be improved to 10 S/m, the sensitivity of the sensor was  $\sim 1.7 \text{ kPa}^{-1}$ , which reveals that the sensitivity can be greatly improved by reducing the initial contact current. For the sensor prepared with 2000# sandpaper, the calculated sensitivity was  $769.2 \text{ kPa}^{-1}$  in the range of 0-2 kPa, while it has a value of  $16.7 \text{ kPa}^{-1}$  in the high-pressure range of 2-18 kPa. In conclusion, CNF/SBS films with a 5% CNF content have optimized electrical properties of CNF/SBS pressure sensors under our experimental conditions.

Due to the limited capability of the SBS/CNF composite to change the resistance, it is difficult to improve the sensitivity to a greater extent by adjusting the intrinsic conductivity of the material. Based on the intrinsic conductive properties of the material, the sensitivity of the sensor is further improved by introducing the surface microstructure of the sensing layer. To further explore the effect of the microstructures of the CNF/SBS film on sensor sensitivity, sandpapers with different grit numbers were used as templates to prepare microstructures of different sizes by the template-stripped method. [Figure 3D](#) clearly shows the effect of microstructure on the sensitivity of the CNF/SBS pressure sensors, revealing that the sensitivity of the sensor decreases with decreasing sandpaper grit numbers. This is mainly because the size of the microstructure depends on the mesh size of the sandpaper. Compared with other different meshes, the 400# mesh of the sandpaper corresponds to the microstructure of the largest size. Under the same pressure load on the sensor, the large size microstructure has fewer contact points than the small size microstructure. Therefore, the pressure is more concentrated in the contact area of the large size microstructure, which will make deformation more likely to occur. Furthermore, sensors with a larger microstructure have a lower contact current in the initial state, which may be responsible for the increase in sensitivity with increasing microstructure.

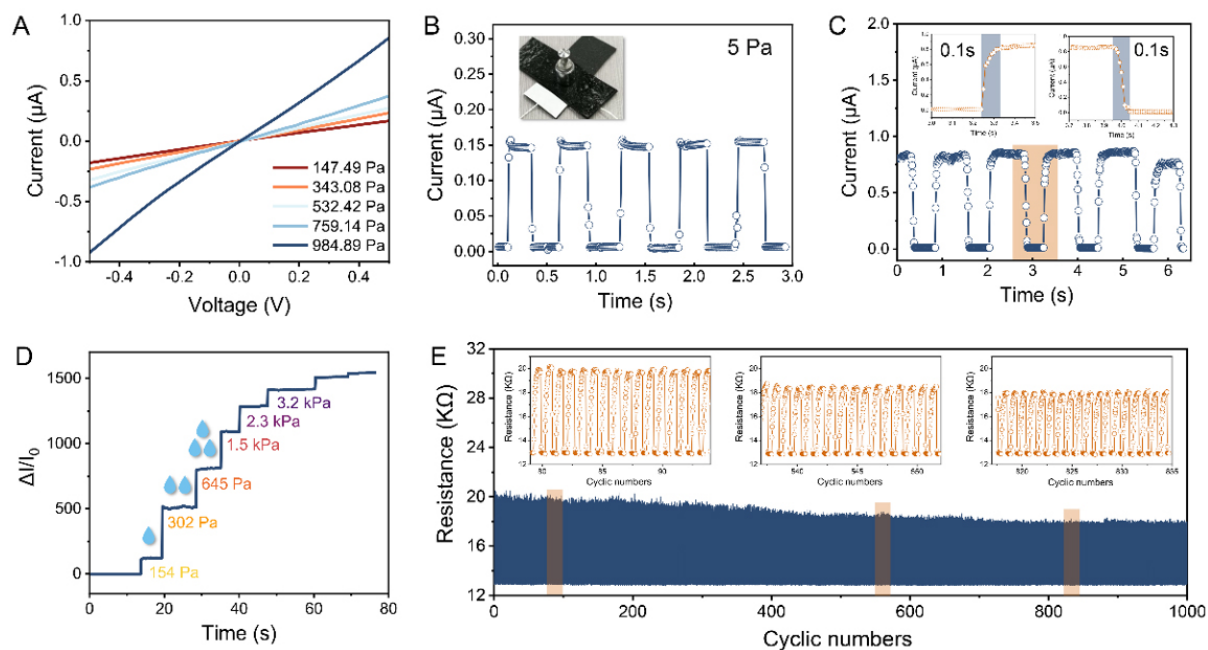


**Figure 4.** (A) I-V behavior of microstructured CNF/SBS film with different pressures; (B) pressure response of microstructure CNF/SBS-based pressure sensor for periodic lowest pressure; (C) response time of microstructure CNF/SBS-based pressure sensor; (D) current variation of microstructure CNF/SBS-based pressure sensor with an applied pressure ranging from 154 Pa to 3.2 kPa; (E) performance of microstructure CNF/SBS-based pressure sensor with cyclic pressure up to 1000 cycles.

In summary, the synergistic effect of material conductivity and surface microstructure can greatly improve the sensitivity and operating range of the sensor. [Figure 3E](#) demonstrates the synergistic process of intrinsic conductivity and microstructure on the resistance change during the deformation process. As the pressure increases, the contact state of the sensor gradually changes from point contact to surface contact. In addition, the contact points of CNF in the SBS matrix gradually increase. Therefore, this synergistic effect of material properties and microstructure leads to the formation of more conductive pathways during compression, thus explaining the effect of pressure on sensitivity.

The additional sensing performance (such as response time, durability and stability) of the highest sensitivity sensor was further evaluated with an electronic universal testing machine and electrochemical workstation. The current-voltage (I-V) curve of the pressure sensor under different pressures is presented in [Figure 4A](#). The applied pressure on the surface of the sensor was constant when the voltage swept from -0.5 to 0.5 V. As the applied pressure increases from 147 Pa to 984 Pa, the slope of the I-V curve increases, meaning that the resistance decreases with increasing pressure and therefore the current also increases. In addition, the linear character of the I-V curves indicated the stability of the sensor resistance, which obeyed Ohm's law. [Figure 4B](#) demonstrates the real-time resistance change of the sensor under loading and unloading pressure, which was achieved by placing and removing a 5 g standard weight (corresponding to a minute pressure of 5 Pa). Repeatable current peaks indicated that the sensor has excellent sensing capabilities for detecting subtle pressures. Response time is also an important performance parameter of pressure sensors. Theoretically, the shorter the response time of a sensor, the weaker the signal hysteresis effect of the sensor. The response and recovery times of the sensor were examined at a cyclic pressure of 1 kPa, as shown in [Figure 4C](#), where the inset shows a sensor response/recovery time of 100 ms.

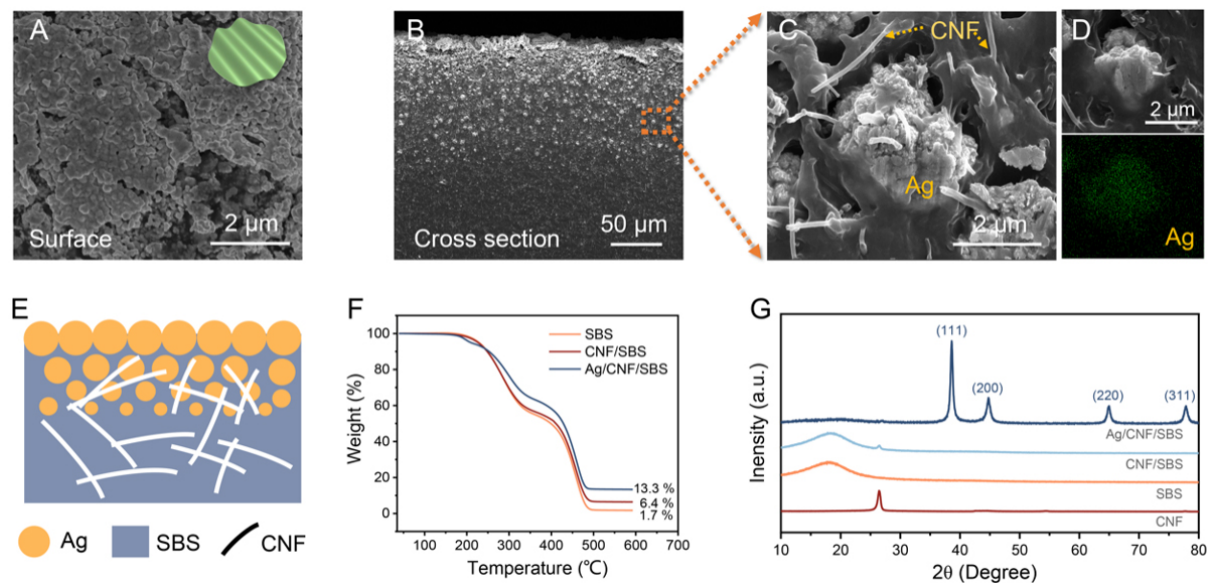


**Figure 5.** (A) SEM image of Ag/CNF/SBS surface; (B) SEM image of Ag/CNF/SBS cross section; (C) characterization of silver particle distribution in CNF/SBS matrix by SEM and EDS; (D) High Magnification SEM image and corresponding EDS mapping image of silver particles in CNF/SBS matrix; (E) Schematic of Ag/CNF/SBS hybrid film structure; (F) thermogravimetric analysis of three samples: SBS; CNF/SBS; Ag/CNF/SBS; (G) XRD patterns of CNF, SBS, CNF/SBS and Ag/SNF/SBS.

A further dynamic response test was conducted by applying stepped pressures on the pressure sensor, leading to the corresponding resistance responses, demonstrating its outstanding pressure identifiability, as shown in [Figure 4D](#). Moreover, the long-term stability of the microstructured CNF/SBS-based pressure sensor was evaluated by cyclic compression for 1000 cycles [[Figure 4E](#)]. When the pressure was applied on the surface of the sensor, the contact resistance was  $\sim 13$  k $\Omega$  and there was almost no change during 1000 cycles, which fully demonstrated the stability of the sensor during the loading pressure cycle test. During the process of unloading pressure, the initial contact resistance of the sensor is gradually reduced, which may be due to the lower Young's modulus of SBS and the relaxation effect. For testing the spatial pressure resolution, both  $2 \times 2$  and  $6 \times 6$  ANF/SBS sensor arrays were fabricated [[Supplementary Figures 2 and 3A](#)]. Three weights (10 g, 20 g, and 100 g) were respectively placed on a  $6 \times 6$  sensor array, as shown in [Supplementary Figure 3B](#). The three-dimensional distribution graph in [Supplementary Figure 3C](#) clarifies that the highest current response was located at the corresponding sites.

Due to the good stretchability of the SBS matrix, a stretching sensor based on a flat CNF/SBS film was designed. When the CNF/SBS-based film is stretched, the conductive network is also stretched, the contacting points of the CNFs decrease and the network within the CNFs is broken, which increases the resistance of the CNF/SBS-based film. Furthermore, in order to further increase the rate of change of resistance of the CNF/SBS-based stretching sensor, Ag NPs were introduced into the shallow surface of the CNF/SBS film by using *in situ* reduction to make the composite material with high conductivity and stretching ability<sup>[39]</sup>.

[Figure 5A](#) shows that the Ag NPs are uniformly reduced and tightly coated on the surface of the CNF/SBS film. It is noteworthy that, unlike conventional chemical plating, the *in situ* reduction method can not only metalize the film surface but also embed Ag nanoparticles inside the CNF/SBS matrix [[Figure 5B and C](#)]. Furthermore, the energy-dispersive X-ray spectroscopy (EDS) result [[Figure 5D](#)], [Supplementary Figure 4](#) and [Supplementary Table 1](#) indicates that the Ag NPs were completely embedded in the CNF/SBS matrix.

As demonstrated in [Figure 5E](#), this unique Ag NP-embedded structure can effectively build the conductive contact point of Ag NPs and CNFs to improve the resistance change during stretching, which can improve the sensitivity of the stretch sensor.

Furthermore, thermogravimetric analysis was performed on SBS, CNF/SBS and Ag/CNF/SBS. As shown in [Figure 5F](#), the results showed that all samples had a significant weight loss at  $\sim 200$  °C, which was due to the oxidation of SBS in air. In addition, the SBS in all samples has been completely oxidized as the temperature was increased to 485 °C. Based on the mass of the remaining residuals, the weight ratios of CNF and Ag NPs in the Ag/CNF/SBS conductive composites can be calculated to be  $\sim 5\%$  and  $\sim 7\%$ , respectively.

Moreover, the SBS, CNF, CNF/SBS and Ag/CNF/SBS were further studied by X-ray diffraction (XRD) to characterize the material components. The obtained XRD patterns are shown in [Figure 5G](#). The diffraction peak at  $2\theta = 17.9^\circ$  corresponds to the amorphous region of SBS. The diffraction peak at  $2\theta = 26.4^\circ$  corresponds to the crystal plane of CNFs. The other four diffraction peaks appearing at  $2\theta = 38.6^\circ$ ,  $44.9^\circ$ ,  $64.9^\circ$  and  $77.9^\circ$  are attributed to the (111), (200), (220) and (311) crystal planes of the face-centered cubic structure of the Ag NPs, respectively.

In order to investigate the performance of the CNF/SBS-based stretching sensors, the tensile mechanical properties [[Figure 6A](#)], resistance-strain characteristics and cyclic stability performance of CNF/SBS and Ag/CNF/SBS were systematically investigated. As shown in [Supplementary Figure 5](#), the Ag/CNF/SBS film was stretched to 400%, which demonstrated its outstanding stretchability and the fact that it holds significant potential as a stretchable sensor. [Figure 6B](#) shows the stress-strain curves of the CNF/SBS film with different mass fractions. As the mass ratio of the CNFs increased from 3% to 5%, the fracture strength of the CNF/SBS composite film gradually increased, but the fracture strain remained greater than 300% [[Figure 6B](#)]. This indicates that modulating the mass ratio of CNFs did not significantly weaken the tensile properties of CNF/SBS. Interestingly, the tensile properties of the Ag/CNF/SBS composite films were significantly improved. Compared with CNF/SBS films, the breaking strength and elongation of Ag/CNF/SBS composite films were doubled to 1.8 MPa and 600%, respectively [[Figure 6C](#)]. This is due to the embedded Ag NPs that not only improve the electrical conductivity of Ag/CNF/SBS by providing more electrical contact points but also greatly enhance the tensile properties of the composite.

Tensile sensitivity is a key parameter of tensile sensors and the effects of CNF mass fraction and Ag NPs on the sensitivity of the CNF/SBS base were studied. Here, the strain is defined as  $\varepsilon = (L - L_0)/L_0$ , where  $L_0$  is the initial length and  $L$  is the length at different elongations and the GF can be calculated by  $GF = (\Delta R/R_0)/\varepsilon$ , where  $\Delta R$ ,  $R_0$  and  $\varepsilon$  are the resistance change, initial resistance and applied strain, respectively. Although the CNF content had little effect on the tensile mechanical properties of CNF/SBS, it had a significant effect on the resistance-strain properties of CNF/SBS [[Figure 6D](#)]. Since the increase in CNF content can significantly improve the conductive pathway of CNF/SBS, it can effectively enhance the working range of CNF/SBS ( $> 300\%$ ). As a result, the CNF/SBS sensor (with a CNF content of 5%) shows a high GF value of 20.6 over a wide working range of 0%-200%, while the GF value was elevated to 6860.9 when the strain was 340%-360%. As mentioned above, both the tensile strength and elongation of the Ag/CNF/SBS composite films were significantly improved after the introduction of Ag NPs. In addition, the GF value (0%-300%) of the Ag/CNF/SBS composite film was also dramatically improved to 105.6, which is five times higher than that of the CNF/SBS film [[Figure 6E](#)]. The Ag/CNF/SBS composite film exhibited an ultrahigh GF of 4646.5 in the higher operating range (500%-600%). As shown in [Figure 6F](#), the Ag NPs distributed on the CNF/SBS surface and in the matrix not only effectively reduce the initial resistance of the stretched sensor but also provide more conductive pathways. Since the CNFs and Ag NPs build a conductive pathway with multiple

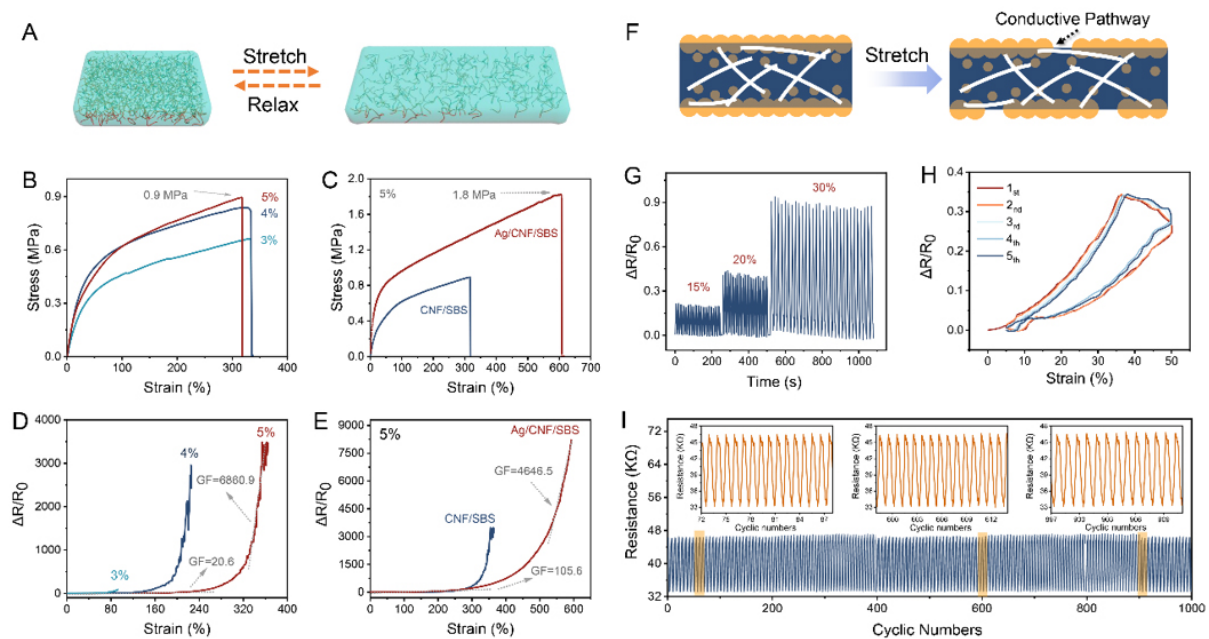


**Figure 6.** (A) Schematic of Ag/CNF/SBS film during stretching and releasing; (B) stress-strain curves of CNF/SBS with different mass fractions; (C) stress-strain curves of CNF/SBS and Ag/CNF/SBS; (D) stress-resistance curve of CNF/SBS tensile sensors of different mass fractions; (E) stress-resistance curve of CNF/SBS and Ag/CNF/SBS; (F) mechanisms of resistance change in Ag/CNF/SBS films during tensile deformation; (G) stretching cycles at different strain rates; (H) strain-dependent normalized resistance of Ag/CNF/SBS under repeated stretching test; (I) cyclic tensile testing of Ag/CNF/SBS-based stretching sensor with a tension strain of 20% for 1000 cycles.

contact points, as the sensor is stretched, the conductive paths constructed by the Ag NPs and CNFs are easily disrupted, the distance between the conductive materials increases and the contact points of CNF and Ag NPs decrease. As a result, the resistance of Ag/CNF/SBS increases significantly due to the disruption of the conductive network and the reduction of the electrical contact points.

The dynamic response of the Ag/CNF/SBS-based strain sensors under stretch/release cycles for 30 cycles with different applied strains (15%, 20% and 30%) is shown in [Figure 6G](#). These stable performances demonstrate that the strain sensors have high reliability and the resistance change is reversible. [Figure 6H](#) shows the  $\Delta R/R_0$ -strain curve for each stretching cycle of the Ag/ANF/SBS strain sensor at a strain of 20%. The cyclic response curve of each cycle in the figure almost overlap, which indicates that the Ag/ANF/SBS strain sensor has good cycling stability. Furthermore, the cyclic stability of the Ag/CNF/SBS film can be up to 1000 under a strain of 20%, as shown in [Figure 6I](#), which indicates the good stability as the strain sensor attached to the human body or robot in monitoring moving signals [[Supplementary Figure 6](#)].

## CONCLUSION

In summary, we fabricated compressible and stretchable sensors based on CNF/SBS. The sensitivity of the flexible pressure sensor ( $769.2 \text{ kPa}^{-1}$ ) was greatly enhanced because of the synergistic effect of the surface microstructure and the intrinsic conductivity of the material. The designed flexible pressure sensor not only exhibited a low-pressure detection limit ( $< 5 \text{ Pa}$ ) and high reliability ( $> 1000$  cycles of compression) but also enabled micro-pressure sensing, such as the detection of pulses and finger flexion. In addition, due to the excellent tensile properties of SBS, the CNF/SBS-based flexible sensor had a total operating range of up to 600% and a maximum linear region GF of 4646.5. Such compressible and stretchable sensors have promising applications in smart and flexible electronic devices for wearable healthcare monitoring

equipment, intelligent robotics and human-machine interfaces.

## DECLARATIONS

### Acknowledgments

Thanks for Taozhao's advice on this study.

### Authors' contributions

Conception and design of the study: Hu Y, Sun R

Performed data analysis and interpretation: Xiong Y, Lin Z, Zhu, P

Performed data acquisition: Xiong Y, Lin Z, Zhao Z, Xu Y, Wan Y

Provided administrative, technical, and material support: Xiong Y, Lin Z

### Availability of data and materials

Not applicable.

### Financial support and sponsorship

This work was financially supported by the National Natural Science Foundation of China (62074154, 61701488, 62101352), Guangdong Basic and Applied Basic Research Fund (2020A1515110962, 2020A1515110154), Shenzhen Science and Technology Program (RCBS20210706092343016, JSGG20210802153000002, JCYJ20210324102208023).

### Conflicts of interest

All authors declared that there are no conflicts of interest.

### Ethical approval and consent to participate

Not applicable.

### Consent for publication

Not applicable.

### Copyright

© The Author(s) 2022.

## REFERENCES

1. Zhang C, Liu S, Huang X, et al. A stretchable dual-mode sensor array for multifunctional robotic electronic skin. *Nano Energy* 2019;62:164-70. [DOI](#)
2. Wang K, Lou Z, Wang L, et al. Bioinspired interlocked structure-induced high deformability for two-dimensional titanium carbide (MXene)/natural microcapsule-based flexible pressure sensors. *ACS Nano* 2019;13:9139-47. [DOI](#) [PubMed](#)
3. Wang C, Xia K, Wang H, Liang X, Yin Z, Zhang Y. Advanced carbon for flexible and wearable electronics. *Adv Mater* 2019;31:e1801072. [DOI](#) [PubMed](#)
4. Tang X, Wu C, Gan L, et al. Multilevel microstructured flexible pressure sensors with ultrahigh sensitivity and ultrawide pressure range for versatile electronic skins. *Small* 2019;15:e1804559. [DOI](#) [PubMed](#)
5. Jung YH, Park B, Kim JU, Kim TI. Bioinspired electronics for artificial sensory systems. *Adv Mater* 2019;31:e1803637. [DOI](#) [PubMed](#)
6. Ding Y, Xu T, Onyilagha O, Fong H, Zhu Z. Recent advances in flexible and wearable pressure sensors based on piezoresistive 3D monolithic conductive sponges. *ACS Appl Mater Interfaces* 2019;11:6685-704. [DOI](#) [PubMed](#)
7. Xia K, Wang C, Jian M, Wang Q, Zhang Y. CVD growth of fingerprint-like patterned 3D graphene film for an ultrasensitive pressure sensor. *Nano Res* 2018;11:1124-34. [DOI](#)
8. Zhang S, Liu H, Yang S, et al. Ultrasensitive and highly compressible piezoresistive sensor based on polyurethane sponge coated with a cracked cellulose nanofibril/silver nanowire layer. *ACS Appl Mater Interfaces* 2019;11:10922-32. [DOI](#) [PubMed](#)
9. Yang JC, Kim JO, Oh J, et al. Microstructured porous pyramid-based ultrahigh sensitive pressure sensor insensitive to strain and

- temperature. *ACS Appl Mater Interfaces* 2019;11:19472-80. DOI PubMed
10. Wang J, Suzuki R, Shao M, Gillot F, Shiratori S. Capacitive pressure sensor with wide-range, bendable, and high sensitivity based on the bionic komochi konbu structure and Cu/Ni nanofiber network. *ACS Appl Mater Interfaces* 2019;11:11928-35. DOI PubMed
  11. Liu S, Li Y, Guo W, et al. Triboelectric nanogenerators enabled sensing and actuation for robotics. *Nano Energy* 2019;65:104005. DOI
  12. Liu Q, Tai H, Yuan Z, Zhou Y, Su Y, Jiang Y. A High-performances flexible temperature sensor composed of polyethyleneimine/reduced graphene oxide bilayer for real-time monitoring. *Adv Mater Technol* 2019;4:1800594. DOI
  13. Li L, Wu S, Li L, et al. Gap-mode excitation, manipulation, and refractive-index sensing application by gold nanocube arrays. *Nanoscale* 2019;11:5467-73. DOI PubMed
  14. Jayathilaka WADM, Qi K, Qin Y, et al. Significance of nanomaterials in wearables: a review on wearable actuators and sensors. *Adv Mater* 2019;31:e1805921. DOI PubMed
  15. Cheng Y, Wu D, Hao S, et al. Highly stretchable triboelectric tactile sensor for electronic skin. *Nano Energy* 2019;64:103907. DOI
  16. Wang C, Ding Y, Yuan Y, et al. Multifunctional, highly flexible, free-standing 3D polypyrrole foam. *Small* 2016;12:4070-6. DOI PubMed
  17. Bae GY, Pak SW, Kim D, et al. Linearly and highly pressure-sensitive electronic skin based on a bioinspired hierarchical structural array. *Adv Mater* 2016;28:5300-6. DOI PubMed
  18. Zhao H, Bai J. Highly sensitive piezo-resistive graphite nanoplatelet-carbon nanotube hybrids/polydimethylsilicone composites with improved conductive network construction. *ACS Appl Mater Interfaces* 2015;7:9652-9. DOI PubMed
  19. Su B, Gong S, Ma Z, Yap LW, Cheng W. Mimosa-inspired design of a flexible pressure sensor with touch sensitivity. *Small* 2015;11:1886-91. DOI PubMed
  20. Park J, Kim M, Lee Y, Lee HS, Ko H. Fingertip skin-inspired microstructured ferroelectric skins discriminate static/dynamic pressure and temperature stimuli. *Sci Adv* 2015;1:e1500661. DOI PubMed PMC
  21. Pang C, Koo JH, Nguyen A, et al. Highly skin-conformal microhairy sensor for pulse signal amplification. *Adv Mater* 2015;27:634-40. DOI PubMed
  22. Wan Y, Qiu Z, Hong Y, et al. A highly sensitive flexible capacitive tactile sensor with sparse and high-aspect-ratio microstructures. *Adv Electron Mater* 2018;4:1700586. DOI
  23. Luo Y, Shao J, Chen S, et al. Flexible capacitive pressure sensor enhanced by tilted micropillar arrays. *ACS Appl Mater Interfaces* 2019;11:17796-803. DOI PubMed
  24. Zhang D, Zhong Y, Wu Y, et al. Liquid metal elastomer with flytrap-inspired pillar structure for stress sensing. *Compos Sci Technol* 2021;216:109066. DOI
  25. Wan Y, Qiu Z, Huang J, et al. Natural plant materials as dielectric layer for highly sensitive flexible electronic skin. *Small* 2018;14:e1801657. DOI PubMed
  26. Wang Z, Zhang L, Liu J, Jiang H, Li C. Flexible hemispheric microarrays of highly pressure-sensitive sensors based on breath figure method. *Nanoscale* 2018;10:10691-8. DOI PubMed
  27. Qiao Y, Jian J, Tang H, et al. An intelligent nanomesh-reinforced graphene pressure sensor with an ultra large linear range. *J Mater Chem A* 2022;10:4858-69. DOI
  28. Cao Y, Li T, Gu Y, Luo H, Wang S, Zhang T. Fingerprint-inspired flexible tactile sensor for accurately discerning surface texture. *Small* 2018;14:e1703902. DOI PubMed
  29. Cho SH, Lee SW, Yu S, et al. Micropatterned pyramidal ionic gels for sensing broad-range pressures with high sensitivity. *ACS Appl Mater Interfaces* 2017;9:10128-35. DOI PubMed
  30. Jung Y, Jung KK, Kim DH, et al. Flexible and highly sensitive three-axis pressure sensors based on carbon nanotube/polydimethylsiloxane composite pyramid arrays. *Sensor Actuat A Phys* 2021;331:113034. DOI
  31. Yang C, Li L, Zhao J, et al. Highly sensitive wearable pressure sensors based on three-scale nested wrinkling microstructures of polypyrrole films. *ACS Appl Mater Interfaces* 2018;10:25811-8. DOI PubMed
  32. Shuai X, Zhu P, Zeng W, et al. Highly sensitive flexible pressure sensor based on silver nanowires-embedded polydimethylsiloxane electrode with microarray structure. *ACS Appl Mater Interfaces* 2017;9:26314-24. DOI PubMed
  33. Ge G, Cai Y, Dong Q, et al. A flexible pressure sensor based on rGO/polyaniline wrapped sponge with tunable sensitivity for human motion detection. *Nanoscale* 2018;10:10033-40. DOI PubMed
  34. Ma Z, Wei A, Ma J, et al. Lightweight, compressible and electrically conductive polyurethane sponges coated with synergistic multiwalled carbon nanotubes and graphene for piezoresistive sensors. *Nanoscale* 2018;10:7116-26. DOI PubMed
  35. Lou Z, Chen S, Wang L, et al. Ultrasensitive and ultraflexible e-skins with dual functionalities for wearable electronics. *Nano Energy* 2017;38:28-35. DOI
  36. Pang Y, Zhang K, Yang Z, et al. Epidermis microstructure inspired graphene pressure sensor with random distributed spinosum for high sensitivity and large linearity. *ACS Nano* 2018;12:2346-54. DOI PubMed
  37. Hu Y, Zhao T, Zhu P, et al. A low-cost, printable, and stretchable strain sensor based on highly conductive elastic composites with tunable sensitivity for human motion monitoring. *Nano Res* 2018;11:1938-55. DOI
  38. Lai J, Zhou H, Jin Z, et al. Highly Stretchable, fatigue-resistant, electrically conductive, and temperature-tolerant ionogels for high-performance flexible sensors. *ACS Appl Mater Interfaces* 2019;11:26412-20. DOI PubMed
  39. Shen Y, Lin Z, Liu X, et al. Robust and flexible silver-embedded elastomeric polymer/carbon black foams with outstanding

electromagnetic interference shielding performance. *Compos Sci Technol* 2021;213:108942. DOI